**FULL TITLE**

Size-tuneable Nanometric MRI Contrast Agents for the Imaging of Molecular Weight Dependent Transport Processes

**AUTHORS NAMES AND AFFILIATION**

Mazen M. El-Hammadi[1], Steven MacLellan[2,3], Christine Dufes[4], William M. Holmes[5], Barrie Condon[5], Ijeoma F. Uchegbu[2] and Andreas G. Schatzlein[2*]

[1]Department of Pharmaceutics and Pharmaceutical Technology, Faculty of Pharmacy, Damascus University, Damascus, Syria;

[2]UCL School of Pharmacy, University College London, 29/39 Brunswick Square, London, UK;

[3]The Doctoral Training Centre, Bioengineering Unit, University of Strathclyde, Glasgow, UK;

[4]Strathclyde Institute of Pharmacy and Biomedical Sciences, University of Strathclyde, Glasgow, UK;

[5]Division of Clinical Neuroscience, University of Glasgow, Glasgow, UK

*Address correspondence to this author at the UCL School of Pharmacy

University College London 29/39 Brunswick Square; London WC1N 1AX

United Kingdom;

Tel: +442077535998;

Fax: +442077535964;

E-mail: a.schatzlein@ucl.ac.uk

**ABSTRACT**

The purpose of the current study was to evaluate size-tuneable polymeric glycol-chitosan (GC)-DTPA Gadolinium (Gd) conjugates as MRI contrast agents that can be used as a platform for imaging of molecular weight (MW) dependent transport processes. GC-DTPA-Gd conjugates of precisely controlled MWs were synthesised and evaluated in mice against Gd-DTPA using time series of high-resolution MRI images of trunk, head, and xenograft flank tumours. GC-DTPA modification ratio was one DTPA per 3.9-5.13 of GC monomers. GC-DTAP-Gd provided overall superior contrast compared to Gd-DTPA with the duration of the enhancement depending on MW (≥1hr for 40kD). The kidneys showed early enhancement also, particularly in the renal pelvis, suggesting renal elimination. Imaging of the head with GC-DTPA-Gd allowed detailed anatomical identification of specific blood vessels in articular with the high MW CA agent. Sequential, high-resolution, isotropic imaging of established A431 xenograft flank tumours with DTPA-Gd and GC-DTPA-Gd demonstrated that the initial distribution of the contrast agents was well correlated with blood vessels and supply. In contrast, subsequent tissue transport was primarily by diffusion and limited by CA molecular weight. The data also highlight the role of heterogeneity in CA distribution which was more prominent for the high MW agent. Precise control of glycol chitosan (GC) polymer chemistry facilitates synthesis of a family of Gd-based MRI contrast agents of tuneable MW but otherwise identical physicochemical properties. Such agents allow isotropic high-resolution three dimensional imaging of MW dependent transport processes relevant to the clinical and pre-clinical prediction of drug transport processes.

**KEYWORDS**

Gadolinium, glycol chitosan, molecular weight, MRI contrast agents.

## 1. INTRODUCTION

Around 50% of magnetic resonance imaging (MRI) studies use contrast agents (CA) such as Gadolinium (Gd) [1], typically administered in a chelated form to avoid the toxicity from free Gd. Most CAs in current clinical use are extracellular fluid agents that distribute readily to all tissues and are typically excreted rapidly by renal filtration due to their low molecular weight (MW) [2]. However, CAs that remain limited to the blood vessels and have an extended plasma half-life are also useful, e.g. for imaging studies of longer duration and imaging of the blood vessels in MR angiography.

Such blood pool CAs would typically require molecular weights large enough to avoid extravasation and ready renal filtration, e.g. by binding of Gd-chelates to albumin (MW 69 kD, 7-8 nm) [3, 4]. Gadofosveset trisodium (Ablavar ®, Bayer Schering Pharma AG) is the first FDA licensed blood pool CA on the market [5]. Blood pool agents provide potential advantages for the visualisation of peripheral vascular pathology, vascular aspects of CNS or kidney disease, and cancer. For example, the progression of solid tumours requires the obligatory activation of the 'angiogenic switch', i.e. the activation of pathways linked to the development of new blood vessels [6]. The developing neovasculature is heterogeneous with atypical morphology, and has reduced hydrodynamic and transport functionality. The discontinuous endothelial lining allows extravasation of macromolecules and nano-sized particulates [7] with a consequent increase in interstitial pressure that hampers nutrient and drug transport into the tumour parenchyma [8] and has been linked to poor prognosis and drug resistance [9]. The effects are thought to be particularly important for the transport of higher MW therapeutics such as anti-bodies, macromolecules, particulate drug carriers, and gene delivery systems [10]. Understanding the impact of MW on transport processes from blood vessels into

tissues thus becomes important not only as a diagnostic feature but also as a potential predictor and biomarker for the transport of such agents in specific tumours. We hypothesised that polymeric MRI CAs of variable MW but identical physicochemical properties could be a useful tool for the study of such molecular weight dependent transvascular transport processes and chose to test this by creating CAs based on glycol chitosan (GC), a versatile biocompatible carbohydrate polymer widely used in the development of nanomedicines and nano-diagnostics.

## 2. MATERIALS AND METHODS

### 2.1. Synthesis of GC-DTPA

All reagents were purchased from Sigma-Aldrich, UK. Glycol chitosan (GC) of varying molecular weight was obtained by acid degradation [11]. Briefly, GC with a degree of polymerisation of 2,500 was degraded (2 hrs, 48 hrs) and recovered by filtration, dialysis, and freeze-drying. The depolymerised GC was then reacted with *p*-SCN-Bn-DTPA (2-(4-isothiocyanatobenzyl)-diethylenetriamine pentaacetic acid, Macrocyclics, USA) in alkaline conditions (24 hrs) and the product obtained after dialysis and freeze-drying (Fig. **1**). The polymer MW was determined by gel permeation chromatography and multi-angle laser light scattering (GPC/ MALLS; Dawn EOS, Wyatt Technology) [11]. 1H-NMR and 1H-1H COSY (Bruker AMX 400 MHZ spectrometer) were performed on GC, *p*-SCN-Bn-DTPA, and GC-DTPA conjugates using deuterated water ($D_2O$). Elemental analysis was carried out on a Thermo Finnigan EA1112 instrument (Thermo Scientific).

### 2.2. Gadolinium Loading

GC-DTPA conjugate and gadolinium (0.5 mmol) were dissolved in imidazole buffer (pH=6.8), mixed and stirred over night to form a precipitate (GC-DTPA-Gd). Phosphate buffer (pH=7) was added to the reaction mixture to redissolve GC-DTPA-Gd and precipitate excess gadolinium. After Gd removal by filtration (0.45 μm) and dialysis the final product was obtained by freeze-drying. The Gd loading of the GC-DTPA polymer was confirmed using isothermal titration calorimetry (ITC), the arsenazo assay, and inductively coupled plasma–atomic emission (ICP-AE): For the ITC (Microcal VP-ITC, MicroCal Inc., USA) Gd chloride hexahydrate (6.5 mM), DTPA, and GC-DTPA (0.2 mM DTPA equivalent) were dissolved (0.1M HCl/NaOH buffer,

pH=2) and de-gassed (ThermoVac, MicroCal Inc., USA). Then aliquots of Gd (20-25 x 5 µL, at 6 min) were injected into the ITC cell filled with either DTPA or GC-DTPA (n=3). Free Gd in solutions of DTPA or GC-DTPA was quantified using the absorbance of a Gd-arsenazo complex (653nm) [12]. The Gd content in a range of samples of GC-DTPA-GD was measured using ICP-AE (138 UL Trace, Jobin Yvon, UK; Vista Pro, Varian Inc.) and Gd standards (0-40mg L-1) at 310nm.

#### *2.2.1. Animal Preparation and Maintenance*

All studies adhered to current national and local regulations and guidelines [13] and were approved by the local ethics committee and the UK authorities. Female nude mice (CD1-nu, ~20g) were anaesthetized (2-3% isofluorane in 70/30 $N_2/O_2$) *via* a facemask. Temperature (maintained at 37 °C using a water jacket), respiration and ECG were monitored using a BIOPAC system (Goleta, CA, U.S.A.). Xenograft tumours, established by subcutaneous injection of $1x10^6$ A431 epidermoid carcinoma cells (ATCC CRL-1555), were used when vascularized (⌀> 5 mm 10+ days).

### 2.3. MR Imaging

All MR imaging was performed on a Bruker Biospin Avance using a 7 T horizontal 30cm bore magnet. In all cases mice were introduced into the bore of the magnetic using a plastic cradle. Trunk imaging was carried out with a 35mm RF resonator coil (gradient maximum 200 mT $m^{-1}$), other images used a Bruker micro-imaging gradient insert (BG-6, 60 mm ID, 100 A amplifier; gradient maximum 1000 mT $m^{-1}$, rise time of 50 µs) or a dedicated optimized tumour solenoid RF micro- coil, built into the animal cradle [14]. The trunk with a focus on the kidneys was imaged using a four slice multi slice multi echo (MSME) 2D sequence with in-plane isotropic voxels 150 × 150 $µm^2$,

slice thickness of 2 mm, in-plane FoV 60 × 34 mm. The sequence (TE=10.5 ms, TR=75 ms, a flip angle of 90° with a 180° re-focusing pulse and four averages) required a total scan time of 1 min 7 sec. The brain was imaged using a 3D FLASH sequence with isotropic voxels 160 × 160 × 160 $\mu m^3$ and a field of view 20 × 16 × 16 $mm^3$. This sequence used an echo time of 3.7 ms, a repetition time of 20 ms, a flip angle of 30°, and one average. The data was visualised using maximum intensity projections (MIPs) in three directions before and after (3 min 20 sec) administration. MIPs technique is an effective way to visualise 3D data sets, which involves constructing a 2D (x,y) image in which each pixel contains the maximum value at that (x,y) location in the third dimension (z). A 3D FLASH sequence was also used to image tumours using isotropic 100 $\mu m^3$ voxels in a field of view of 8 x 8 x 8 $mm^3$ with an echo time of 3.5 ms, a repetition time of 25.0 ms, a flip angle of 30°, and either two or four averages with total scan times of 5 min 20 sec and 10 min 40 sec, respectively. Tumour angiography studies used a multi-slice 2D time of flight (TOF) gradient echo sequence sliced perpendicular to the axis of the coil or sagittal in anatomical terms with isotropic 100 $\mu m^3$ voxels in-plane resolution and 60 sequential slices of 100 μm thickness. The echo time used was 5 ms and the recovery time was 40 ms with 8 averages. Scans of trunk, head and tumour were performed on different animals. In addition, MRI studies using GC-DTPA-Gadolinium conjugates and Gd-DTPA were carried out following the injection of the contrast agents to the same animal, separated by an adequate washout period. Raw data was exported as free induction decay (FID) file and then processed using Interactive
Data Language (IDL, RSI, Boulder, Colorado, U.S.A.) routines.

## 3. RESULTS

### 3.1. GC-DTPA Synthesis

The acid degradation of glycol chitosan reduces the polymer MW in a nonlinear manner following a first order reaction with a first order rate constant of –1.35 ($Mn=94448\ e^{-1.346t} + 7041$, $r^2=0.99$) [15]. The molecular weight of the resultant polymer can be selected based on the choice of reaction conditions, in particular reaction time and temperature [15]. The reaction produces polymers of low polydispersity (Mw/Mn ~1.07-1.3) with a yield inversely proportional to the degradation time (49-75%, low MW polymer is lost in dialysis) and a weight average MW of 37.8±1.4 kDa (GC40), 16.6±1.6 kDa (GC16) and 12.3±1.9 kDa (GC12), respectively. The yield of the GC-DTPA conjugation step was 61-86% with the freeze-dried product obtained as an off-white/yellow cotton like product. The NMR analysis confirms the product and very low N-acetylation levels (< 0.05 mol% at 2.0 ppm, Fig. **1**). Signals from the polymer and DTPA overlap but the benzene group at δ7.3-7.5 indicates the presence of the benzyl isothiocyanate moiety of *p*-SCN-Bn-DTPA. Furthermore, a new peak for the GC anomeric proton becomes detectable at 4.4ppm, presumably as a result of conformational changes of the polymer. The conjugation level of GC-DTPA was measured using elemental analysis, an arsenazo III assay, and ITC. Based on the elemental nitrogen and sulphur the number of GC monomers per DTPA pendant group was calculated as 5.15 (GC40-DTPA), 3.96 (GC16-DTPA), and 4.89 (GC12-DTPA), respectively (Table **1**). Gd3+ ions bind to arsenazo III to form the colorimetrically detectable complex (log K = 15.85 [12]) only once DTPA has been saturated with Gd to form the DTPA-Gd complex (log K = 22.46 [16]). The colorimetric Gd arsenazo III complex thus allows measurement of free and GC-DTPA chelated Gd from which the level of conjugation (GC moles/DTPA

moles) was determined to be 4.83 (GC40-DTPA), 3.94 (GC16-DTPA), and 5.37 (GC12-DTPA), respectively (Table **1**). ITC was used to measure heat enthalpy of the GC-DTPA/Gd3+ interactions for GC16-DTPA and to determine the conjugation level by comparison with free DTPA and Gd (Fig. **2**). At the acidic pH used in this experiment (pH=2), the carboxylic groups of DTPA are protonated (un-ionised) and interactions with $Gd^{3+}$ occur at a slower rate. Initial Gd injections produce large peaks resulting from the binding of Gd3+ to DTPA. As the concentration of free DTPA reduces the heat reduces to the heat of dilution represented by the small peaks at the end of the curve. The stoichiometry of binding (GC16-DTPA:Gd) was used to calculate the GC:DTPA molar ratio which was of 3.79±0.05. The yield for the off-white to yellow freeze-dried product was 217 mg (GC40-DTPA-Gd) and 120mg (GC16-DTPA-Gd), respectively. The average ratio (ICPAES) of Gd per mg of GC-DTPA-Gd was 0.079±0.003 mg for GC40-DTPA-Gd, 0.100±0.005 mg for GC16-DTPA-Gd, and 0.073±0.005 mg for GC12-DTPA-Gd.

### 3.2. Magnetic Resonance Imaging Results

The initial biodistribution was imaged over 29 min post the intravenous administration of GC16-DTPA-Gd (0.1 mmole Gd $kg^{-1}$). The MR imaging of the trunk showed very clearly highlighted kidneys when compared to the pre-administration image (Fig. **3**). Immediately after injection detailed imaging shows GC40-DTPA-Gd and GC12-DTPA-Gd in the kidneys with rapid passage to renal pelvis and then ureter. Although the level of contrast decreased over time, the kidneys remained highlighted. Magnevist, when administered at the same dose of Gd, yielded only low level of dynamic contrast enhancement (Fig. **3**). Renal enhancement has been suggested as being indicative of contrast agent removal from the blood and elimination by the

kidneys [17]. The higher molecular weight GC40-DTPA-Gd continued to be present in the kidney for a longer period of time (≥30 min) suggesting a longer plasma residence time consistent with a larger polymer MW. The data suggest these CAs are filtered in a MW dependent fashion by the kidneys and eliminated in the urine.

When a very short TR is used (as in this study), the effect of the contrast agent on T1 relaxation time diminishes unless the agent exhibits a high relaxivity or is present at a high concentration at the site of interest, or both. This explains the higher contrast in GC-DTPA-Gd images resulting from the increased relaxivity of the polymer-based contrast agents when compared to Magnevist. The imaging properties of Magnevist, GC40-DTPA-Gd, and GC12-DTPA-Gd were compared further by imaging the cranium (Fig. **4**). In contrast to Magenvist, GC40-DTPA-Gd remains confined to the blood pool giving a much clearer enhancement of the brain vasculature while GC12-DTPA-Gd shows an intermediate effect. This blood pool selectivity dramatically changes the structures and detail that can be visualised from the volume data as shown by Maximum Intensity Projections (MIPs) (Fig. **4**). These visualise regions with a level of enhancement greater than 20% based on the differential between preinjection and post-injection contrast (t=3 min 20 sec). The CAs show a distinct distribution with signal time profiles dependent on anatomical location. Regions of interest (ROI) representing brain parenchyma, blood vessels, and surrounding tissue were identified and signal intensities compared over time (Fig. **5**). All CAs show a sharp initial enhancement in the major blood vessel. While both Magnevist and GC12- DTPA-Gd show a brief peak, the higher MW GC40-DTPAGd shows a sustained enhancement suggesting a prolonged plasma half-life compared to the lower MW agents. However, the signal decay at one hour suggests signal intensities would reach pre-contrast levels within two hours. Both polymeric CAs GC40-DTPA-

Gd and GC12-DTPA-Gd do not enhance contrast in the brain parenchyma or the surrounding connective tissue (Fig. **5 b** and **c**). Conversely the connective tissue region shows the greatest enhancement and longest time to peak when imaged with Magnevist, suggestive of a diffusion dependent accumulation (Fig. **5a**). The vascular contrast enhancement using the GC40-DTPA-Gd is sufficient to allow anatomical identification of specific larger blood vessels using regional maximum intensity projections. Based on the differential contrast of the high and low MW polymers these CAs were applied to the investigation of molecular weight dependent transport processes in solid tumours. Transport limitations of individual tumours were visualised by sequential imaging of low and high MW CAs administered to the same animal and same tumour, separated by a washout period (Fig. **6**). For both agents initial delivery to the tumour was correlated with blood supply. As would be expected the lower molecular weight material exhibited greater diffusion and consequently covered a larger area of the tumour. A volume projection highlights the overall disparity in tumour coverage of the two agents. The heterogeneity of distribution relates to identifiable anatomical structural detail but is also linked to the difference in CA molecular weight.

## 4. DISCUSSION

Molecular weight is one of the key factors determining biological behaviour of macromolecules in terms of biodistribution, and vascular and tissue transport. Here we explore the use of biocompatible polymers with defined and tailored molecular weights as the basis of a family of MRI CAs to explore these processes by MRI. Such CAs, having the same physical chemistry but different molecular weights, could be adapted to serve preferentially as blood pool CAs or to study macromolecular transport processes. The potential for polymer- based CAs with enhanced blood residence time has previously been explored. When poly-L-lysine-GTPA of increasing MW were explored as potential blood pool agents it has previously been shown that plasma half-life is increased and renal clearance reduced with increasing MW [18]. However, agents such as carboxy methyl dextran–GTPA have limited utility in exploring MW dependent processes because of their broad MW distribution (10-163 kD) [19]. On the other hand, CAs with a defined molecular structure, such as dendrimers, possess monodisperse MWs but do not easily allow continuous tuning of polymer molecular weight [20]. Using CAs with shared chemical structure and physical chemistry but different MW minimises the risk of variable interactions with biological macromolecules. Such binding would potentially lead to changes in relaxivity thus complicating direct comparisons. MW is not only a key determinant of a CAs potential utility as a blood pool agent but can also be used to assess pathological transport processes. Once tumours are able to induce the growth of new vasculature (angiogenic switch) they may proliferate and metastasise. The developing ‘leaky’ vasculature allows extravasation of macromolecules that leads to an increase in interstitial pressure leading to diffusion (or perfusion) limited transport

into the tumour parenchyma which affects low MW drugs [21] but even more higher MW therapeutics such as anti-bodies, macromolecules particulate drug carriers, gene delivery systems [10], and which has been linked to poor prognosis and drug resistance [9]. MRI has been applied to understand and quantify such transport processes, in particular by applying DCE-MRI and associated mathematical derivation of parameters such as transfer co-efficient, vascular volume fraction and measures of permeability and perfusion, typically applying models based on the unidirectional transfer of contrast material between compartments such as the Tofts two compartment model [22] and the three-compartment model [23]. The current study analyses the relationships between blood supply and contrast agent delivery directly and in high resolution.

The data emphasises the important role of underlying anatomical structures and local tissue heterogeneity in determining the detailed spatiotemporal distribution of molecules of different molecular weight. The concept of using MRI contrast agents as surrogates for drugs to investigate tumour delivery and transport issues itself is not new. Both low molecular weight contrast materials [24] and macromolecular contrast materials [25] have been used to predict the delivery and transport of drugs of a similar molecular weight. In both cases the delivery of the drug, confirmed by histology, proved to be well correlated with the prediction by MRI.

Furthermore, studies have been performed in which contrast agents with different molecular weights have been serially administrated to the same tumour in order to optimise modelling procedures [26, 27]. The studies reported here would appear to be the first time to show that these two concepts (the use of contrast agents as drug surrogates and the serial administration of contrast agents with different molecular weights) could be brought together. Here we synthesised and characterised GC-

DTPA-$Gd^{3+}$ as a biocompatible macromolecular contrast agent for which the molecular weight can be tuned precisely for various imaging purposes. We demonstrate its utility as a blood pool agent by detailed imaging of mouse brain vascular architecture, show that filtration *via* the kidney provides early and sustained contrast enhancement in the kidney, and provide evidence that GC-DTPA-Gd of high and low MW can be used to characterise molecular weight dependent transport in murine xenograft tumours with a high spatial and temporal resolution. The imaging also shows that the diffusion (or perfusion) distances for higher molecular weight materials were lower than for low molecular weight materials. Data from doxorubicin treated breast cancers demonstrate that heterogeneity in drug distribution at the histological level can persist for many hours [21] but work in experimental tumours suggests that vascular supply can also change rapidly over time [28]. Our data highlights the potential role of such transport differences for the heterogeneity of drug exposure and subsequent resistance in tumours, in particular with respect to drug MW.

## CONCLUSION

Precise control of glycol chitosan polymer chemistry facilitates synthesis of Gd-based MRI contrast agents with defined molecular weights which allow isotropic high resolution three-dimensional imaging of the heterogeneity of molecular weight dependent transport processes, in particular in tumours, in order to understand and potentially predict effects on therapy. Studies of this type using a series of well calibrated CAs, differing only by MW, could potentially provide a surrogate biomarker for accessibility and transport of drug treatments in tumours. In drug development terms this may also help in the selection of a suitable tumour models to test new high MW treatments.

## CONFLICT OF INTEREST

The authors confirm that this article content has no conflicts of interest.

## ACKNOWLEDGEMENTS

AGS acknowledges support by Tenovus Scotland.

## REFERENCES


[1] Bellin MF, Van der Molen AJ. Extracellular gadolinium-based contrast media: An overview. Eur J Radiol 2008; 66(2): 160-7.

[2] Geraldes CFGC, Laurent S. Classification and basic properties of contrast agents for magnetic resonance imaging. Contrast Media Mol Imaging 2009; 4(1): 1-23.

[3] Schmiedl U, Ogan MD, Moseley ME, Brasch RC. Comparison of the contrast-enhancing properties of albumin-(Gd-DTPA) and Gd- DTPA at 2.0 T: And experimental study in rats. AJR Am J Roentgenol 1986; 147(6): 1263-70.

[4] Barrett T, Kobayashi H, Brechbiel M, Choyke PL. Macromolecular MRI contrast agents for imaging tumor angiogenesis. Eur J Radiol 2006; 60(3): 353-66.

[5] Chopra A, Shan L, Eckelman WC, *et al*. Molecular imaging and contrast agent database (MICAD): Evolution and progress. Mol Imaging Biol 2012; 14(1): 4-13.

[6] Hanahan D, Folkman J. Patterns and emerging mechanisms of the angiogenic switch during tumorigenesis. Cell 1996; 86(3): 353-64.

[7] Hashizume H, Baluk P, Morikawa S, *et al*. Openings between defective endothelial cells explain tumor vessel leakiness. Am J Pathol 2000; 156(4): 1363-80.

[8] Heldin CH, Rubin K, Pietras K, Ostman A. High interstitial fluid pressure - an obstacle in cancer therapy. Nat Rev Cancer 2004;4(10): 806-13.

[9] Minchinton AI, Tannock IF. Drug penetration in solid tumours. Nat Rev Cancer 2006; 6(8): 583-92.

[10] Pluen A, Boucher Y, Ramanujan S, *et al*. Role of tumor-host interactions in interstitial diffusion of macromolecules: Cranial *vs*. subcutaneous tumors. Proc Natl Acad Sci USA 2001; 98(8): 4628-33.

[11] Wang W, McConaghy AM, Tetley L, Uchegbu IF. Controls on polymer molecular weight may be used to control the size of palmitoyl glycol chitosan polymeric vesicles. Langmuir 2001; 17(3): 631-6.

[12] Gouin S, Winnik FM. Quantitative assays of the amount of diethylenetriaminepentaacetic acid conjugated to water-soluble polymers using isothermal titration calorimetry and colorimetry. Bioconjug Chem 2001; 12(3): 372-7.

[13] Workman P, Aboagye EO, Balkwill F, *et al*. Guidelines for the welfare and use of animals in cancer research. Br J Cancer 2010; 102(11): 1555-77.

[14] Holmes WM, Maclellan S, Condon B, *et al*. High-resolution 3D isotropic MR imaging of mouse flank tumours obtained *in vivo* with solenoid RF micro-coil. Phys Med Biol 2008; 53(2): 505-13.

[15] Lalatsa A, Garrett NL, Ferrarelli T, Moger J, Schatzlein AG, Uchegbu IF. Delivery of peptides to the blood and brain after oral uptake of quaternary ammonium palmitoyl glycol chitosan nanoparticles. Mol Pharm 2012; 9(6): 1764-74.

[16] Cacheris WP, Nickle SK, Sherry AD. Thermodynamic study of lanthanide complexes of 1,4,7-triazacyclononane-N,N',N''-triacetic Acid and 1,4,7,10-tetraazacyclododecane-N,N',N'',N'''-tetraacetic acid. Inorg Chem 1987; 26(6): 958-60.

[17] Li Z, Li W, Li X, Pei F, Li Y, Lei H. The gadolinium complexes with polyoxometalates as potential MRI contrast agents. Magn Reson Imaging 2007; 25(3): 412-7.

[18] Vexler VS, Clement O, Schmitt-Willich H, Brasch RC. Effect of varying the molecular weight of the MR contrast agent Gd-DTPApolylysine on blood

pharmacokinetics and enhancement patterns. J Magn Reson Imaging 1994; 4(3): 381-8.

[19] Siauve N, Clement O, Cuenod CA, Benderbous S, Frija G. Capillary leakage of a macromolecular MRI agent, carboxymethyldextran-Gd-DTPA, in the liver: pharmacokinetics and imaging implications. Magn Reson Imaging 1996; 14(4): 381-90.

[20] Sato N, Kobayashi H, Hiraga A, *et al*. Pharmacokinetics and enhancement patterns of macromolecular MR contrast agents with various sizes of polyamidoamine dendrimer cores. Magn Reson Med 2001; 46(6): 1169-73.

[21] Lankelma J, Dekker H, Luque FR, *et al*. Doxorubicin gradients in human breast cancer. Clin Cancer Res 1999; 5(7): 1703-7.

[22] Tofts PS, Kermode AG. Measurement of the blood-brain barrier permeability and leakage space using dynamic MR imaging. 1. Fundamental concepts. Magn Reson Med 1991; 17(2): 357-67.

[23] Pathak AP, Artemov D, Ward BD, Jackson DG, Neeman M, Bhujwalla ZM. Characterizing extravascular fluid transport of macromolecules in the tumor interstitium by magnetic resonance imaging. Cancer Res 2005; 65(4): 1425-32.

[24] Artemov D, Solaiyappan M, Bhujwalla ZM. Magnetic resonance pharmacoangiography to detect and predict chemotherapy delivery to solid tumors. Cancer Res 2001; 61(7): 3039-44.

[25] Kobayashi H, Shirakawa K, Kawamoto S, *et al*. Rapid accumulation and internalization of radiolabeled herceptin in an inflammatory breast cancer xenograft with vasculogenic mimicry predicted by the contrast-enhanced dynamic MRI with the macromolecular contrast agent G6-(1B4M-Gd)(256). Cancer Res 2002; 62(3): 860-6.

[26] Turetschek K, Preda A, Novikov V, *et al*. Tumor microvascular changes in antiangiogenic treatment: Assessment by magnetic resonance contrast media of different molecular weights. J Magn Reson Imaging 2004; 20(1): 138-44.

[27] Orth RC, Bankson J, Price R, Jackson EF. Comparison of single and dual-tracer pharmacokinetic modeling of dynamic contrast enhanced MRI data using low, medium, and high molecular weight contrast agents. Magn Reson Med 2007; 58(4): 705-16.

**[28]** Debbage PL, Griebel J, Ried M, Gneiting T, DeVries A, Hutzler P. Lectin intravital perfusion studies in tumor-bearing mice: Micrometer-resolution, wide-area mapping of microvascular labeling, distinguishing efficiently and inefficiently perfused microregions in the tumor. J Histochem Cytochem 1998; 46(5): 627-39.

## FIGURE LEGENDS

**Table 1.** Characteristics of GC-DTPA conjugates and level of conjugation, represented by number of GC monomers per DTPA pendant group, measured using elemental analysis, arsenazo III assay, and ITC.

**Fig. (1).** Structure, reaction scheme, and annotated 1H-NMR spectra of GC-DTPA in D2O indicating the presence of the benzylisothiocyanate moiety of p-SCN-Bn-DTPA at □7.3-7.5.

**Fig. (2).** Determination of the conjugation level of GC-DTPA/Gd3+ based on the measurement of heat enthalpy. Injection of Gd3+ (6.5 mM) into a buffered aqueous solution of GC16-DTPA (0.2 mM based on p-SCN-Bn-DTPA, 25 oC and pH = 2) yields a titration curve showing heat flow against amount of injected Gd3+(top) and of enthalpy versus molar ratio (bottom).

**Fig. (3).** Time course of trunk MR of mice imaged over 28 min and injected with Magnevist (top panel) and GC40-DTPA-G at 0.1 mmole Gd.kg-1 (bottom panel). The polymer CAs shows an enhanced level of contrast over a significantly prolonged duration compared to Magnevist as well as early enhancement of the kidney parenchyma and renal pelvis.

**Fig. (4).** MR imaging of a mouse head after administration of (**a**) Magnevist, (**b**) C12-DTPA-Gd, and (**c**) GC40-DTPA-Gd. Left panel: Maximum intensity projections of the cranium in the coronal, sagittal, and transverse planes prior and 3 mins 20 sec after administration of CAs. Middle panel: Volume projections showing areas of greater

than 20% enhancement demonstrate the different levels of vascular retention of the agents. Right panel: Maximum intensity projections of murine brain imaged using GC40-DTPA-Gd allow visualisation of cranial vasculature in sufficient to allow anatomical identification of blood vessels (1-Superior sagittal sinus; 2-Lateral superior cerebellar artery; 3-Common carotid artery; 4-Posterior cerebral artery).

**Fig. (5).** MR images and time dependent contrast intensity profiles of the mouse cranium imaged using (**a**) Magnevist, (**b**) GC12-DTPA-Gd, and (**c**) GC40-DTPA-Gd. A number of specific anatomical regions of interest (ROI) were identified (red = brain parenchyma, blue = brain blood supply, green & turquoise = tissue surrounding the brain). The contrast intensity in those structures was then extracted from the 4D data stack and plotted over time yielding intensity-time curves.

**Fig. (6).** Comparison of molecular weight dependent contrast enhancement in a tumour. A431 epidermoid carcinoma flank tumour in a mouse imaged over a period of 20 min after intravenous administration of first Magnevist followed by GC40-DTPA-Gd (top panel). Changes in the distribution between low (Magnevist) and high MW CA (GC40-DTPA-Gd) between 0 to 10 min and 10 to 20 min are visualised, respectively (bottom panel, left). High and low MW agent distribution 20 min after injection in the same tumour is visualised as a volume projection of CA distribution (bottom right panel).

Table 1

| Conjugate | Degradation (hours) | MW (kDa) | GC:DTPA (mol:mol) | Conjugation level[a] | | | |
|---|---|---|---|---|---|---|---|
| | | | | Elemental analysis | Arsenazo assay III | ITC | Average |
| GC40-DTPA | 2 | 37.8±1.4 | 01:02 | 5.15 | 4.83±0.14 | n/a | 4.99 |
| GC16-DTPA | 48 | 16.6±1.6 | 01:01 | 3.96 | 3.94±0.19 | 3.79±0.05 | 3.9 |
| GC12-DTPA | 48 | 12.3±1.9 | 01:02 | 4.89 | 5.37±0.06 | n/a | 5.13 |

[a]GC monomers per DTPA pendant group.

Figure 1

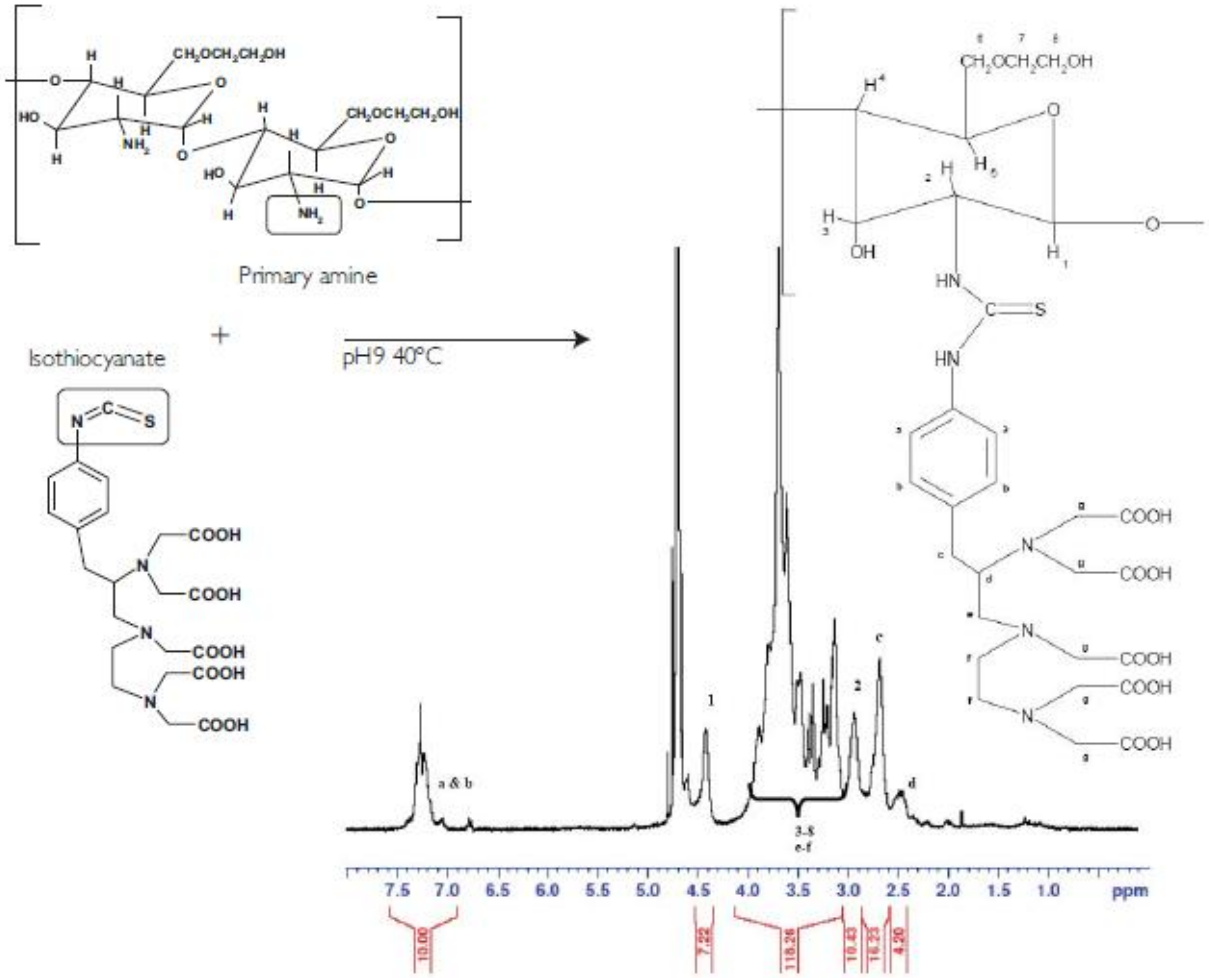
Primary amine
+
Isothiocyanate
pH9 40°C
COOH
HN
C
S
a & b
1
2
c
d
3.8
e-f
7.5 7.0 6.5 6.0 5.5 5.0 4.5 4.0 3.5 3.0 2.5 2.0 1.5 1.0 ppm
10.00
7.22
118.26
16.43
16.23
4.20

Figure 2

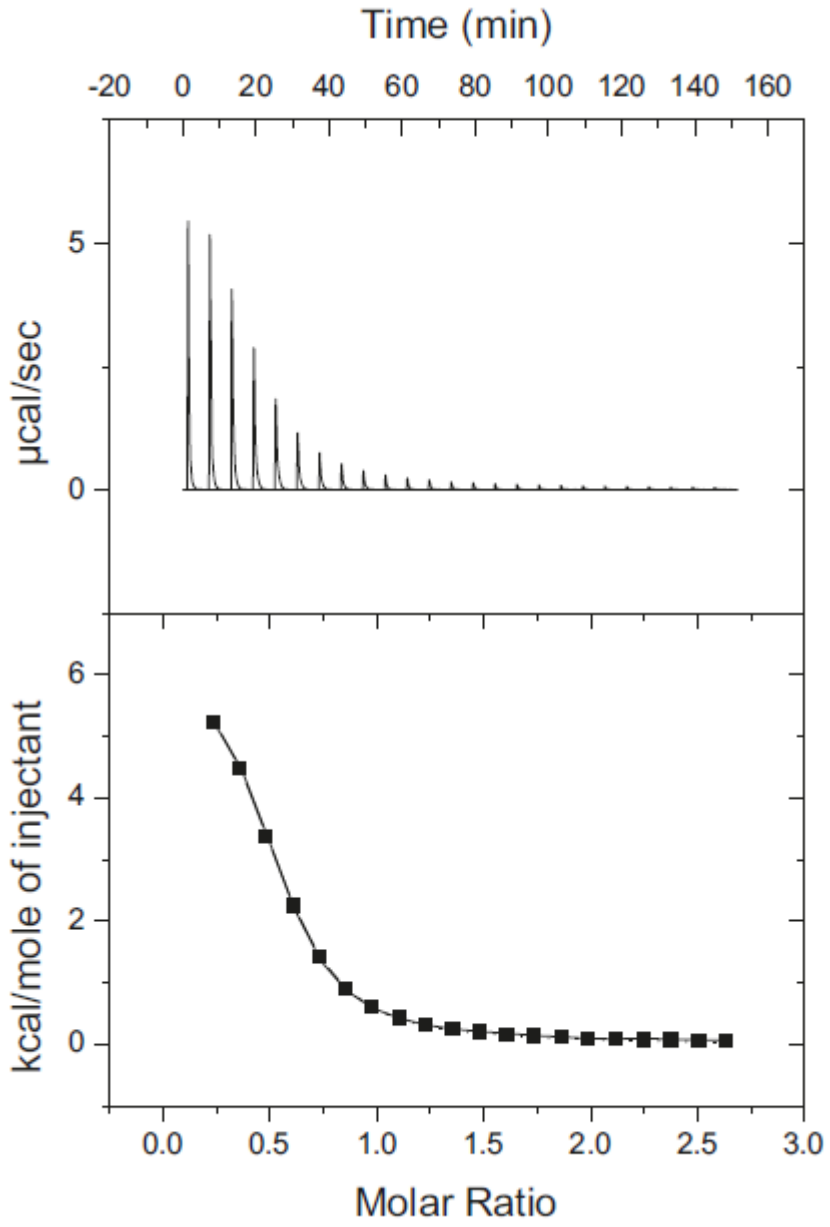
Time (min)
-20
0
20
40
60
80
100
120
140
160
µcal/sec
5
0
kcal/mole of injectant
6
4
2
0
0.0
0.5
1.0
1.5
2.0
2.5
3.0
Molar Ratio

Figure 3

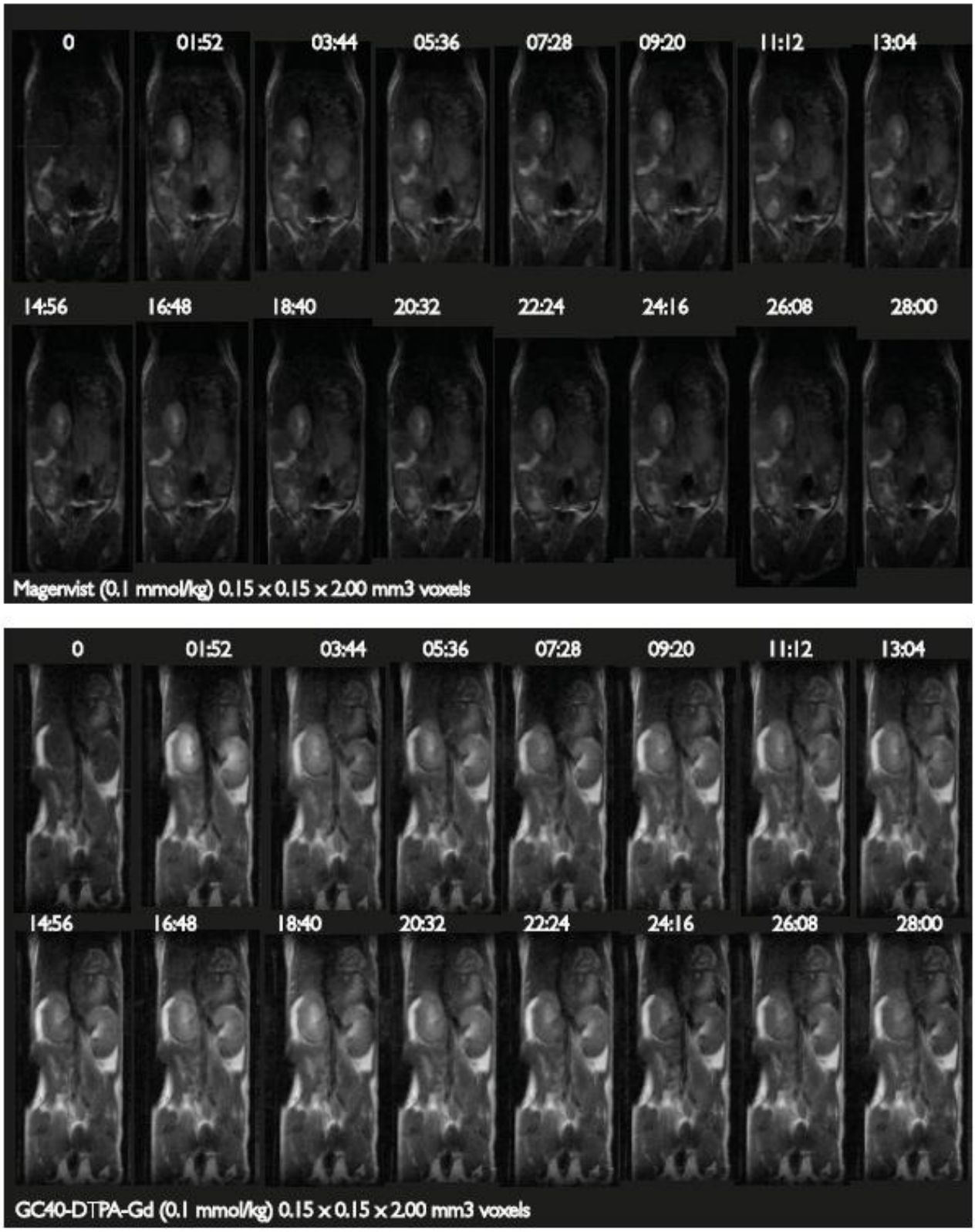
0
01:52
03:44
05:36
07:28
09:20
11:12
13:04
14:56
16:48
18:40
20:32
22:24
24:16
26:08
28:00
Magenvist (0.1 mmol/kg) 0.15 x 0.15 x 2.00 mm3 voxels
0
01:52
03:44
05:36
07:28
09:20
11:12
13:04
14:56
16:48
18:40
20:32
22:24
24:16
26:08
28:00
GC40-DTPA-Gd (0.1 mmol/kg) 0.15 x 0.15 x 2.00 mm3 voxels

Figure 4

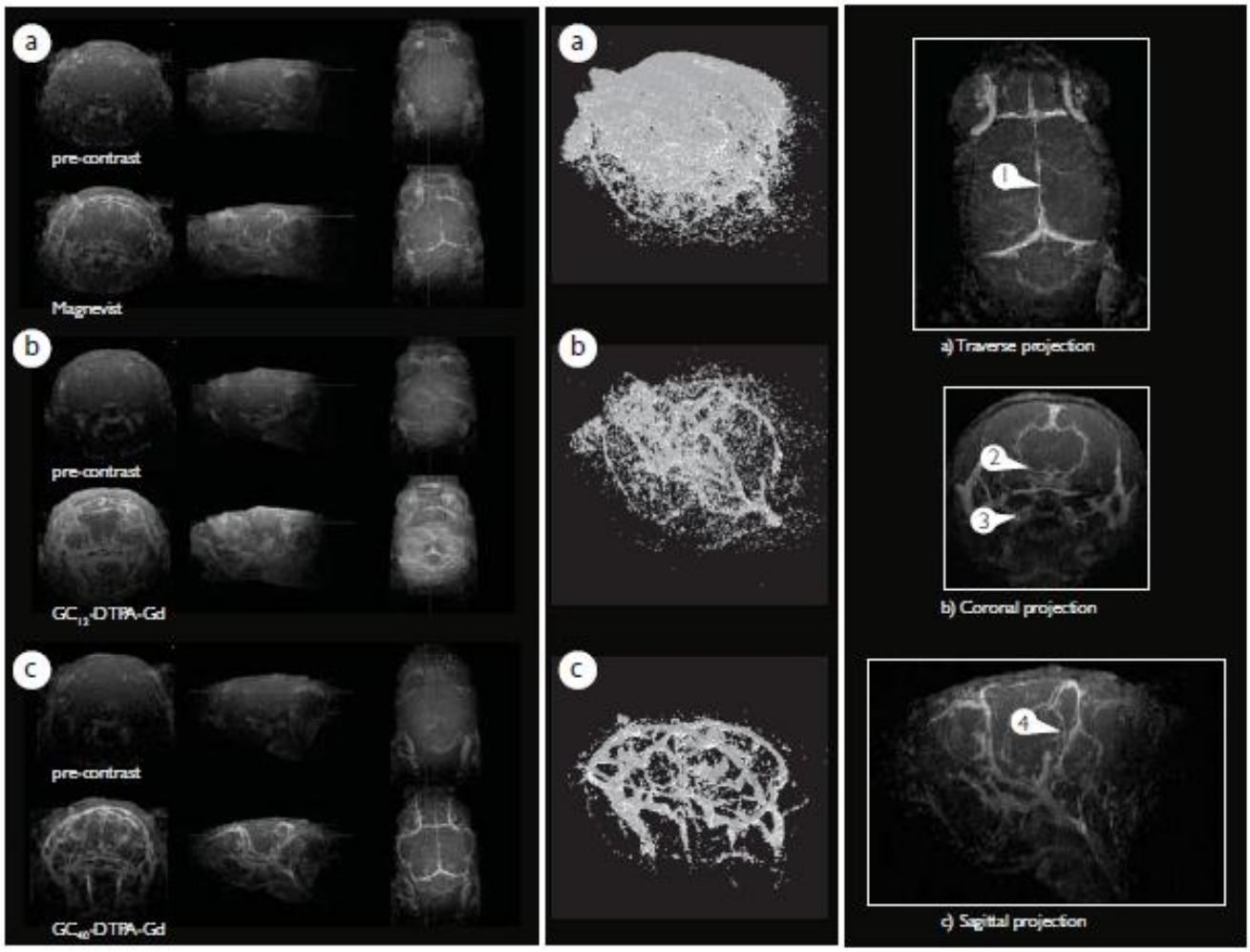
a
pre-contrast
Magnevist
b
pre-contrast
GC12-DTPA-Gd
c
pre-contrast
GC48-DTPA-Gd
a
b
c
1
a) Traverse projection
2
3
b) Coronal projection
4
c) Sagittal projection

Figure 5

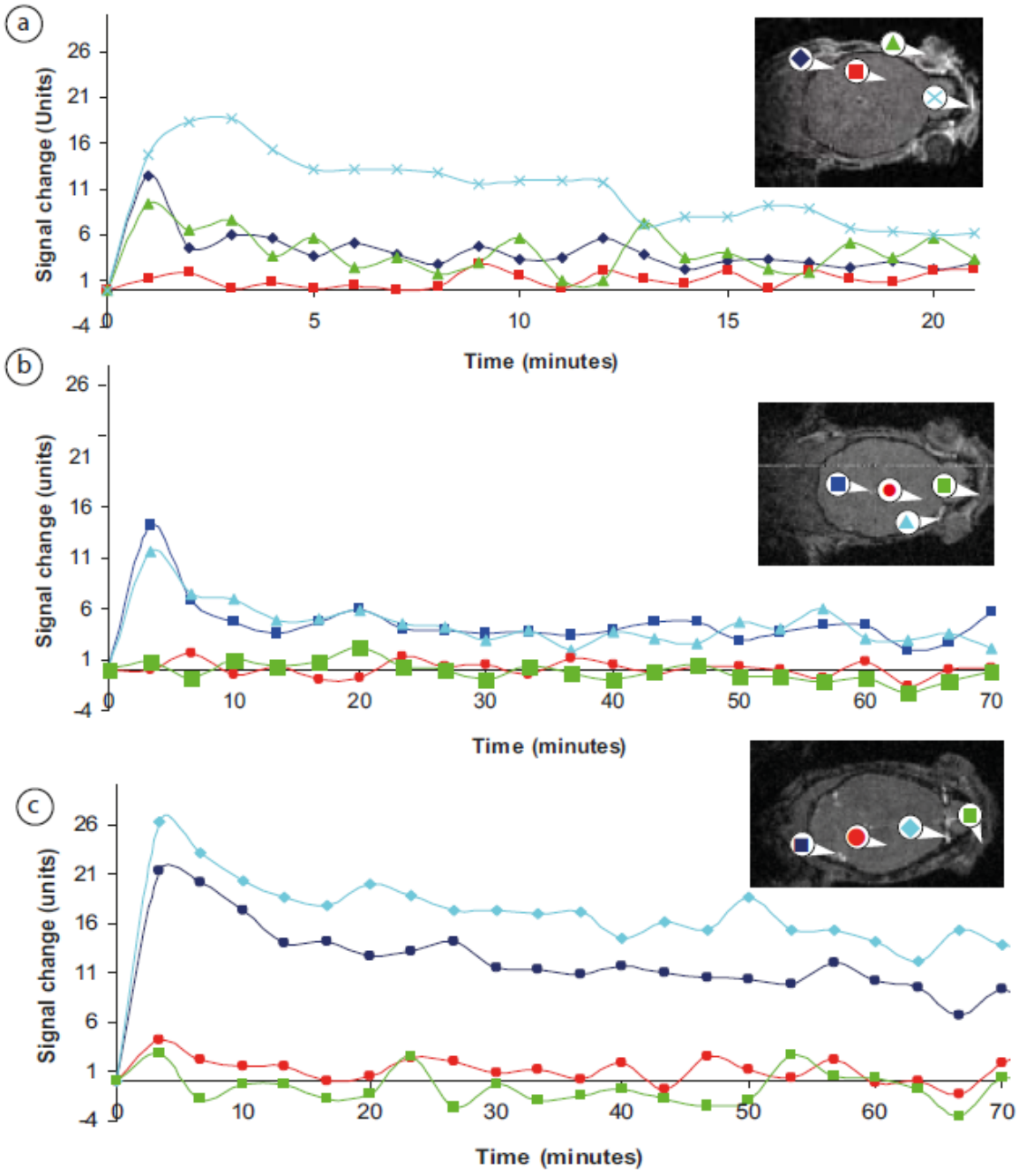
a
Signal change (Units)
26
21
16
11
6
1
-4
0
5
10
15
20
Time (minutes)
b
Signal change (units)
26
21
16
11
6
1
-4
0
10
20
30
40
50
60
70
Time (minutes)
c
Signal change (units)
26
21
16
11
6
1
-4
0
10
20
30
40
50
60
70
Time (minutes)

Figure 6

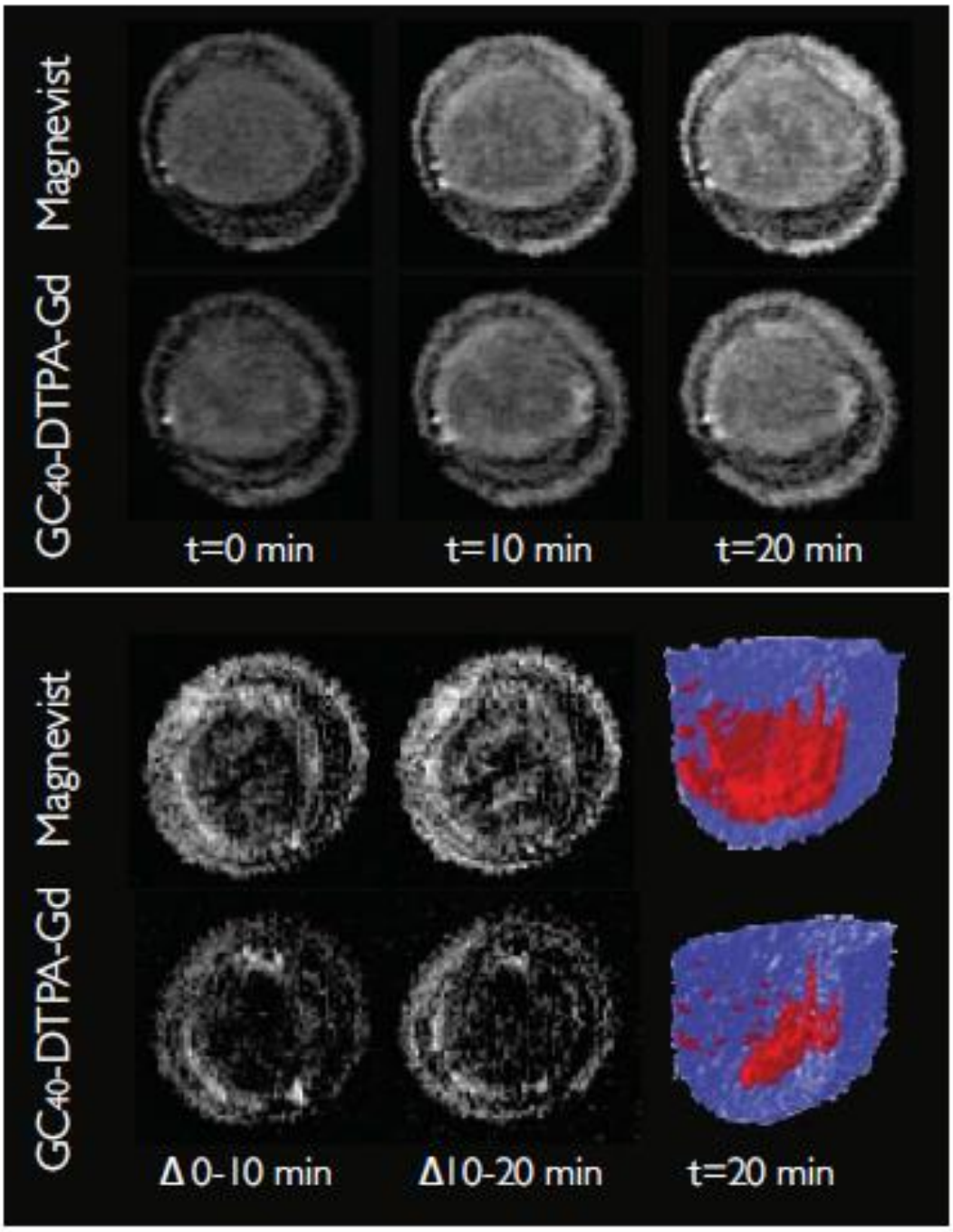
Magnevist
GC40-DTPA-Gd
t=0 min
t=10 min
t=20 min
Magnevist
GC40-DTPA-Gd
Δ0-10 min
Δ10-20 min
t=20 min